The Astrophysical Journal Letters, 912:L1 (6pp), 2021 May 1 https://doi.org/10.3847/2041-8213/abf56e

High H_0 Values from CMB E-mode Data: A Clue for Resolving the Hubble Tension?

Graeme E. Addison
Dept. of Physics & Astronomy, The Johns Hopkins University, 3400 N. Charles St., Baltimore, MD 21218-2686, USA; gaddison@jhu.edu
Received 2021 January 29; revised 2021 April 2; accepted 2021 April 6; published 2021 April 28

Abstract

The E-mode (EE) CMB power spectra measured by Planck, ACTPol, and SPTpol constrain the Hubble constant to be 70.0 ± 2.7, $72.4^{+3.9}_{-4.8}$, and $73.1^{+3.3}_{-3.9}$ km s^{-1} Mpc^{-1} within the standard ΛCDM model (posterior mean and central 68% interval bounds). These values are higher than the constraints from the Planck temperature (TT) power spectrum, and consistent with the Cepheid-supernova distance ladder measurement $H_0 = 73.2 \pm 1.3$ km s^{-1} Mpc^{-1}. If this preference for a higher value was strengthened in a joint analysis it could provide an intriguing hint at the resolution of the Hubble disagreement. We show, however, that combining the Planck, ACTPol, and SPTpol EE likelihoods yields $H_0 = 68.7 \pm 1.3$ km s^{-1} Mpc^{-1}, 2.4σ lower than the distance ladder measurement. This is due to different degeneracy directions across the full parameter space, particularly involving the baryon density, $\Omega_b h^2$, and scalar tilt, n_s, arising from sensitivity to different multipole ranges. We show that the E-mode ΛCDM constraints are consistent across the different experiments within 1.4σ, and with the Planck TT results at 0.8σ. Combining the Planck, ACTPol, and SPTpol EE data constrains the phenomenological lensing amplitude, $A_L = 0.89 \pm 0.10$, consistent with the expected value of unity.

Unified Astronomy Thesaurus concepts: Cosmic microwave background radiation (322); Hubble constant (758); Observational cosmology (1146)

1. Introduction

The standard Lambda-Cold Dark Matter (ΛCDM) cosmological model is supported by a range of observations, including fluctuations in the cosmic microwave background (CMB), the large-scale distribution of galaxies, and, with the exception of lithium-7, primordial element abundance (e.g., Bennett et al. 2013; Planck Collaboration VI 2020; Fields et al. 2020; eBOSS Collaboration 2020). A significant disagreement has emerged between ΛCDM constraints and more direct measurements of the Hubble constant, H_0. Combining Planck CMB data with baryon acoustic oscillation (BAO) measurements yields $H_0 = 67.61 \pm 0.44$ km s^{-1} Mpc^{-1} (eBOSS Collaboration 2020), while the latest Cepheid-supernova distance ladder result is 73.2 ± 1.3 km s^{-1} Mpc^{-1} from the Supernova H_0 for the Equation Of State team (SH0ES; Riess et al. 2021). The SH0ES result is supported by various partially or fully independent low-redshift observations (e.g., Kourkchi et al. 2020; Schombert et al. 2020; Wong et al. 2020; Soltis et al. 2021; Blakeslee et al. 2021). Some low-redshift analyses have yielded lower values, consistent with both the CMB+BAO value and the SH0ES result (e.g., Freedman et al. 2019; Birrer et al. 2020). The "low" values of H_0 based on measurements sensitive to the physics in the early universe are not driven by any single data set or observational method (e.g., Aubourg 2015; Addison et al. 2018).

CMB data play a critical role in constraining possible deviations from ΛCDM, including modifications introduced in an attempt to address the H_0 disagreement (e.g., Knox & Millea 2020, and references therein). Future improvements in cosmological constraints from the CMB will largely come from polarization. The Planck temperature-polarization (TE) cross-spectrum already constrains ΛCDM parameters with a comparable precision to the temperature (TT) spectrum, for example, $H_0 = 68.44 \pm 0.91$ km s^{-1} Mpc^{-1} from TE+lowE, and 66.88 ± 0.92 km s^{-1} Mpc^{-1} from TT+lowE, where "lowE" denotes the E-mode polarization likelihood at $\ell < 30$, which primarily constrains the optical depth, τ (Planck Collaboration VI 2020).

Ongoing and upcoming ground-based surveys including Advanced ACTPol (Henderson et al. 2016), SPT-3G (Benson et al. 2014), Simons Observatory (Ade et al. 2019), and CMB-S4 (Abazajian et al. 2019), will make increasingly precise measurements of the EE spectrum, ultimately aiming to achieve uncertainties dominated by signal (sample variance) in the damping tail out to $\ell \simeq 3000$–5000. By this point, the E-mode polarization will be more constraining than the temperature fluctuations, both for ΛCDM parameters like H_0, and additional parameters constrained from the damping tail, such as the effective number of relativistic species, $N_{\rm eff}$ (e.g., Galli et al. 2014, Section 4 of Ade et al. 2019).

Parameter uncertainties from current EE spectra from Planck, the Atacama Cosmology Telescope (ACT) ACTPol receiver (Thornton et al. 2016), and the South Pole Telescope (SPT) SPTpol camera (Austermann et al. 2012) are fairly large, with H_0 constrained to 4%–6% precision for each survey (Henning et al. 2018; Aiola et al. 2020; Planck Collaboration VI 2020). Recently, Dutcher et al. (2021) reported the first cosmological constraints from the SPT-3G receiver. Assuming ΛCDM, they found a preference for a higher H_0 from the EE spectrum (76.4 ± 4.1 km s^{-1} Mpc^{-1}) than Planck TT. They pointed out that the EE results from Planck, ACTPol, SPTpol, and SPT-3G individually exhibit this same trend (see their Figure 13). The EE spectra mildly prefer higher H_0 values than the Planck TT data, and also their TE counterparts.

Is this trend made more significant by combining the EE spectra from the different surveys? If so, it could be hinting at some modification to ΛCDM that addresses the Hubble tension while impacting temperature and polarization results differently. Such a hint would be valuable since the low-redshift H_0 measurements provide very little direction for physical resolutions of the disagreement. Alternatively, statistically significant shifts in parameters from EE compared to TT could

Table 1
Posterior Mean and Central 68% ΛCDM Parameter Constraints from Fitting to EE Spectra, Including in Each Case the $\ell < 30$ Planck lowE Likelihood to Constrain τ, with H_0 Reported in km s^{-1} Mpc^{-1}

EE Data	$100\Omega_b h^2$	$\Omega_c h^2$	$100\theta_{\rm MC}$	$10^9 A_s e^{-2\tau}$	n_s	H_0
Planck	2.40 ± 0.12	$0.1157^{+0.0043}_{-0.0047}$	$1.04000^{+0.00087}_{-0.00086}$	1.905 ± 0.024	$0.980^{+0.013}_{-0.015}$	70.0 ± 2.7
ACTPol	$2.27^{+0.12}_{-0.14}$	0.108 ± 0.011	$1.0409^{+0.0015}_{-0.0016}$	$1.92^{+0.21}_{-0.20}$	$0.986^{+0.053}_{-0.060}$	$72.4^{+3.9}_{-4.8}$
SPTpol	2.25 ± 0.12	$0.1055^{+0.0077}_{-0.0076}$	1.0408 ± 0.0016	1.722 ± 0.068	$1.029^{+0.038}_{-0.048}$	$73.1^{+3.3}_{-3.9}$
Planck+ACTPol	$2.274^{+0.061}_{-0.062}$	0.1187 ± 0.0032	1.03988 ± 0.00068	1.884 ± 0.022	$0.9663^{+0.0100}_{-0.0101}$	67.8 ± 1.6
Planck+SPTpol	2.314 ± 0.060	0.1165 ± 0.0030	1.03997 ± 0.00075	1.877 ± 0.021	0.975 ± 0.010	68.9 ± 1.5
ACTPol+SPTpol	$2.268^{+0.082}_{-0.083}$	$0.1070^{+0.0057}_{-0.0056}$	$1.04087^{+0.00101}_{-0.00099}$	$1.762^{+0.059}_{-0.060}$	$0.998^{+0.028}_{-0.032}$	$72.6^{+2.3}_{-2.6}$
Planck+ACTPol+SPTpol	2.287 ± 0.048	0.1167 ± 0.0027	$1.04002^{+0.00061}_{-0.00060}$	1.869 ± 0.020	0.9700 ± 0.0094	68.7 ± 1.3

indicate some new systematic issue that needs to be understood moving forward.

In this work we reexamine constraints from the Planck, ACTPol, and SPTpol EE data[1] to shed light on this issue, motivated by both parameter tensions and the importance of the EE measurements for the future of CMB cosmology. We describe the public data sets and codes used in this work in Section 2, present results in Section 3, and conclude in Section 4. The main results are shown in Table 1 and Figure 1.

2. Data and Model Fitting

We perform cosmological parameter fitting using Markov Chain Monte Carlo (MCMC) sampling implemented in the CosmoMC[2] package (Lewis & Bridle 2002; Lewis 2013). Theoretical CMB power spectra are computed from parameters using CAMB[3] (Lewis et al. 2000; Howlett et al. 2012). The ΛCDM parameters varied in the fits are the physical baryon and cold dark matter densities, $\Omega_b h^2$ and $\Omega_c h^2$, the CosmoMC parameter $\theta_{\rm MC}$, which is closely related to the angular spacing of the acoustic peaks, the scalar amplitude, A_s, the optical depth, τ, and the scalar tilt, n_s. The value of H_0 at each step in the chain is then derived from these. We follow the assumptions used by Planck Collaboration VI (2020) for massive neutrinos (fixing sum of masses to 0.06 eV), the connection between primordial helium abundance and $\Omega_b h^2$, and the parametric "tanh" form for the evolution of the ionization fraction at reionization.

The Planck and ACTPol teams have released multiple likelihood versions. In this work we use the likelihoods used to compute the main results reported by these collaborations. For Planck we use the plik likelihood at $\ell \geqslant 30$, and the lowE likelihood at $\ell < 30$. These likelihoods are described by Planck Collaboration V (2020) and available on the Planck Legacy Archive.[4] For ACTPol we use the public ACTPollite likelihood described by Choi et al. (2020) and Aiola et al. (2020).[5] For SPTpol we use the public likelihood provided by Henning et al. (2018).[6] Foreground and nuisance parameters are varied in the fits using priors recommended by each collaboration and marginalized over in all results provided in this work. The overall calibration of the Planck, ACTPol, and SPTpol spectra, and associated uncertainties, are discussed in Section 3.3.4 of Planck Collaboration V (2020), Section 7 of Choi et al. (2020), and Section 4.5 of Henning et al. (2018), respectively. Convergence of the fits is assessed using multiple chains following the standard CosmoMC approach, requiring the Gelman-Rubin diagnostic of within-chain and across-chain parameter spread, $R - 1 < 0.01$ (Gelman & Rubin 1992).

3. Results

3.1. Results from Each Experiment Separately.

We present results from fitting ΛCDM to the Planck, SPTpol, and ACTPol EE spectra in Table 1. We provide the posterior mean plus bounds of the central 68% interval. Since the constraint on τ is largely driven by the Planck $\ell < 30$ lowE likelihood in each case we report the combination $A_s e^{-2\tau}$ rather than A_s and τ separately (Kosowsky et al. 2002). Figure 1 shows two-dimensional contours containing 68 and 95% of the posterior distributions for each experiment. In the figure we show H_0 instead of $\theta_{\rm MC}$ to facilitate comparison with low-redshift measurements.

We remark here that, for all three experiments separately, n_s lies within 1.5σ of unity, and H_0 differs by at most 1.1σ from the latest SH0ES measurement of 73.2 ± 1.3 km s^{-1} Mpc^{-1} (Riess et al. 2021).

3.2. Results from Combining Experiments

We show results for ΛCDM parameters from a joint fit to the Planck, ACTPol, and SPTpol EE spectra in Table 1 and Figure 1.

Combining the three EE spectra does not reinforce the preference for higher values of H_0 from the individual fits, yielding $H_0 = 68.7 \pm 1.3$ km s^{-1} Mpc^{-1} (posterior mean and central 68% interval). This value lies 2.4σ lower than the distance ladder measurement 73.2 ± 1.3 km s^{-1} Mpc^{-1} (Riess et al. 2021). This is the main result of this paper, and is due to the different degeneracy directions in the full multidimensional ΛCDM parameter space, and the fact that there are offsets in the preferred mean values from each experiment (even though, as discussed in Section 3.3, below, they are statistically consistent).

To help illustrate this, we include dashed lines in Figure 1 corresponding to H_0 of 73 km s^{-1} Mpc^{-1} and n_s of 0.99. These values are allowed within the 68% contours of each individual experiment but disfavored at around 3σ in the combination. Looking at the $n_s - \Omega_b h^2$ panel of Figure 1 we see that these parameters are positively correlated for Planck EE, but

[1] At the time of writing, the SPT-3G likelihood from Dutcher et al. (2021) is not publicly available, although we expect the SPT-3G and SPTpol results to produce similar constraints when combined with Planck (see Section 3.2).
[2] https://cosmologist.info/cosmomc/
[3] https://camb.info/
[4] http://pla.esac.esa.int/pla/
[5] https://lambda.gsfc.nasa.gov/product/act/act_dr4_likelihood_get.cfm
[6] https://pole.uchicago.edu/public/data/henning17/ and https://lambda.gsfc.nasa.gov/product/spt/sptpol_lh_2017_get.cfm

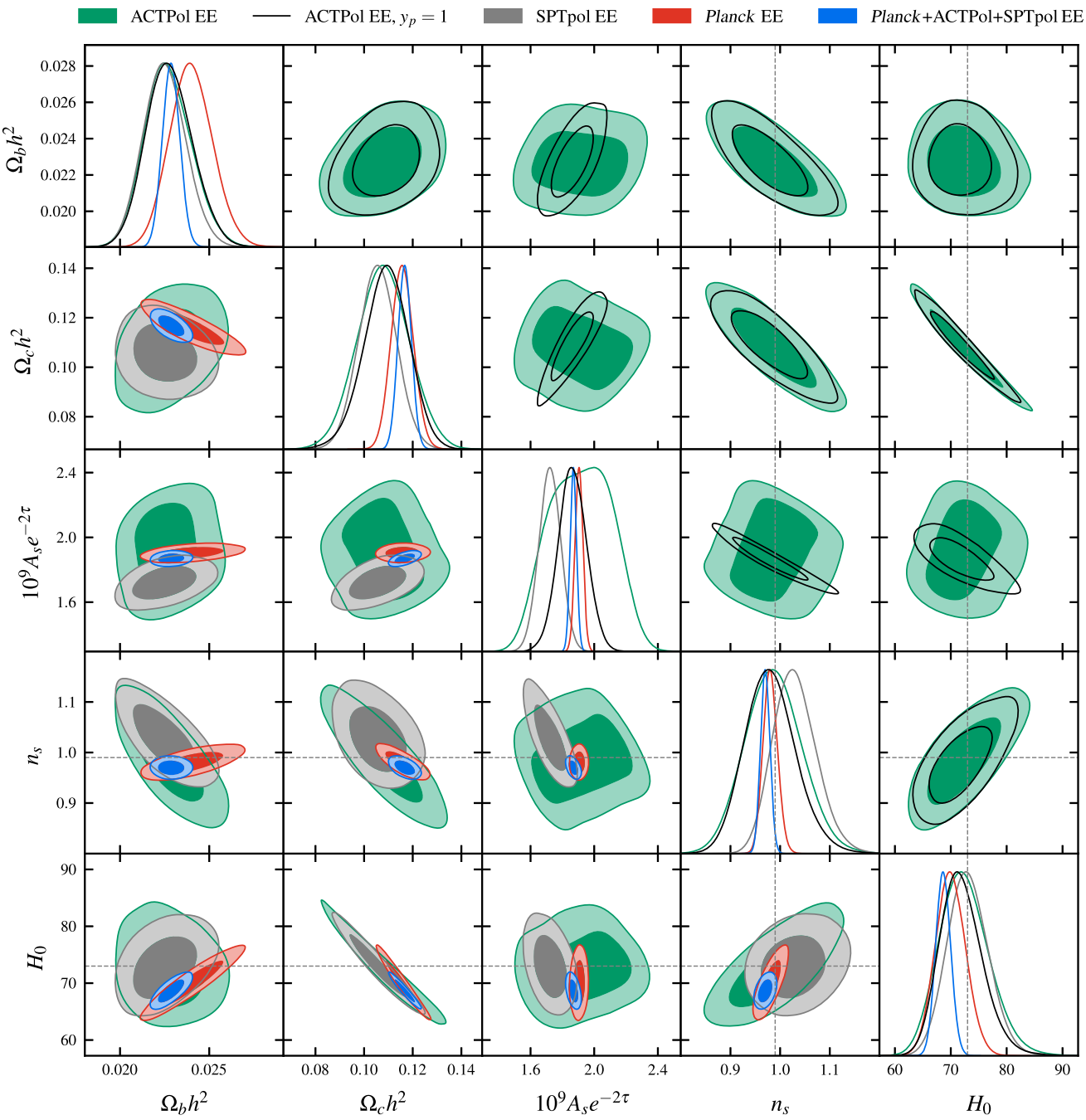

Figure 1. Lower triangle: contours containing 68% and 95% of the posterior distribution from fits to EE power spectra in ΛCDM. Combining the Planck, ACTPol, and SPTpol EE spectra does not reinforce the preference for higher values of H_0 from the data sets individually, due to different degeneracy directions, for example, in the $n_s - \Omega_b h^2$ plane. Dashed lines at $H_0 = 73$ km s^{-1} Mpc^{-1} and $n_s = 0.99$ correspond to a point in parameter space that is allowed within the 68% contours of each experiment individually but disfavored at 3σ in the combination. Each constraint includes the Planck `lowE` likelihood to constrain τ. Upper triangle: effect of fixing the ACTPol polarization efficiency parameter, y_p, as discussed in Section 3.3.2.

negatively correlated for ACTPol and SPTpol. While the experiments individually prefer or allow higher n_s values, with correspondingly higher H_0, this is not possible in the combination because a consensus must also be reached for $\Omega_b h^2$. The portion of multidimensional parameter space most acceptable to all the data sets instead features lower H_0 and n_s values.

Most of the Planck EE spectrum constraining power is at larger angular scales ($\ell \lesssim 600$), where, for pivot scale $k_p = 0.05$ Mpc^{-1}, increasing n_s leads to an overall suppression of power. The ACTPol and SPTpol EE constraining power is mostly from finer scales, where increasing n_s leads to an overall enhancement of power. The Planck, ACTPol, and SPTpol EE bandpowers are shown in Figure 8 of Dutcher et al. (2021). This difference in behavior leads to a significant change in the $n_s - \Omega_b h^2$ degeneracy direction because the derivative of the theory spectrum with respect to $\Omega_b h^2$ also changes sign between larger and smaller angular scales (Figure 1 of Galli et al. 2014). A similar change in the $n_s - \Omega_b h^2$ degeneracy direction is also apparent over different multipole ranges of the TT spectrum (e.g., Figure 1 of Addison et al. 2016). These changes in degeneracy directions are reproduced in Fisher

Table 2
Consistency of ΛCDM Parameters from different EE Spectra, Using Test Described in Section 3.3

EE Data Sets	Overall	Worst 1-D
Planck vs ACTPol	1.0σ	0.7σ ($\Omega_b h^2$)
Planck vs SPTpol	1.2σ	2.5σ ($A_s e^{-2\tau}$)
ACTPol vs SPTpol	0.7σ	1.3σ ($A_s e^{-2\tau}$)
Planck vs ACTPol+SPTpol	1.4σ	2.2σ ($A_s e^{-2\tau}$)
Planck+ACTPol vs SPTpol	0.9σ	2.2σ ($A_s e^{-2\tau}$)
Planck+SPTpol vs ACTPol	0.9σ	0.8σ ($\Omega_c h^2$)

forecasts, without using the actual measured power spectra, although where exactly the different contours intersect in parameter space is, of course, determined by the measurements.

As a point of comparison, a simple inverse variance weighting of the one-dimensional H_0 constraints from Planck, ACTPol, and SPTpol, ignoring the parameter correlations, yields $71.4 \pm 1.9\,\mathrm{km\,s^{-1}\,Mpc^{-1}}$. The reduction in the uncertainty in the full multidimensional fit illustrates this complementarity of the lower and higher multipoles of the EE spectrum for breaking parameter degeneracies.

While we do not yet have access to the SPT-3G EE likelihood, we note that the SPT-3G and SPTpol two-dimensional ΛCDM parameter contours exhibit similar degeneracy directions (Figure 9 of Dutcher et al. 2021). We therefore expect the combination of Planck and SPT-3G to produce similar results to the Planck+SPTpol or Planck+ACTPol results in Table 1, including a lower value of H_0 and n_s than reported for SPT-3G EE alone.

3.3. Consistency of Different EE Spectra within ΛCDM

In this subsection we quantify the consistency of the Planck, ACTPol, and SPTpol EE results within ΛCDM. Provided the data sets are independent and the posterior parameter distributions are well approximated as multivariate Gaussian[7] we can perform a simple χ^2 test for the consistency of the difference of the posterior means with zero (e.g., Addison et al. 2016; Raveri & Hu 2019),

$$\chi^2_{12} = \sum_{ij} (\mu_{1,i} - \mu_{2,i})(C_{11} + C_{22})^{-1}_{ij}(\mu_{1,j} - \mu_{2,j}). \quad (1)$$

Here the data sets are labeled with subscripts 1 and 2, the Roman subscripts label parameters, and μ and C are the mean and covariance estimated from the MCMC chains. This χ^2 is converted to an equivalent Gaussian "$N\sigma$" by matching the probability-to-exceed from the χ^2 distribution to that from a standard Gaussian distribution but considering only positive values (so $\chi^2 = 0$ corresponds to 0σdifference). These $N\sigma$ values are reported in Table 2. Based on calculations using subsets of the full MCMC chains, the finite number of steps used to estimate C sets an uncertainty floor of around 0.1σ in this test. Since the τ posteriors are driven by the common `lowE` likelihood we perform a comparison in five dimensions[8], $\{\Omega_b h^2, \Omega_c h^2, \theta_{\rm MC}, A_s e^{-2\tau}, n_s\}$, following, for example, Aiola et al. (2020) and Dutcher et al. (2021).

[7] We discuss these assumptions in Sections 3.3.1 and 3.3.2.

[8] Substituting H_0 for $\theta_{\rm MC}$ in these tests impacts the consistency results at $<0.1\sigma$.

In addition to testing the consistency between each pair out of Planck, ACTPol, and SPTpol, we tested the consistency between each experiment and the combination of the other two. These results are also shown in Table 2. Overall we find no significant evidence for disagreement, with parameter differences no larger than 1.4σ. This indicates that the preference for the lower H_0 value in the combined fit cannot be attributed to any significant tensions between the separate EE data sets.

The most notable single parameter difference is in $A_s e^{-2\tau}$ for SPTpol, which falls 2.5σ low of Planck EE. The SPTpol polarization maps were calibrated by comparing the SPTpol and SPTpol×Planck EE spectra on the SPTpol patch (Section 7.3 of Henning et al. 2018). This 2.5σ difference may therefore simply arise from an unfortunate statistical fluctuation on the SPTpol patch, but could also hint at some systematic issues arising when reanalyzing Planck data on small sky patches (see also Section 13.3 of Choi et al. 2020). Given the low statistical significance we do not attempt to investigate this issue further in this work. The SPT-3G data produced $A_s e^{-2\tau}$ constraints in better agreement with Planck (Figure 9 of Dutcher et al. 2021), although this is not surprising given the calibration was performed against the full-sky Planck spectra in that analysis.

3.3.1. Independence of EE Spectra from Different Experiments

In reality the different data sets are correlated with one another due to partial sky overlap. Due to a combination of current EE noise levels and the small size of the SPTpol patch we argue below that we can safely neglect these correlations (as done in previous studies).

The covariance between the parameters from the Planck and ACTPol EE spectra was estimated by Aiola et al. (2020) under the assumption that the E-modes measured by ACTPol are a subset of the modes accessible to the Planck analysis. Aiola et al. (2020) found that ignoring the covariance would artificially tighten parameter constraints from a joint EE fit only at the percent level (i.e., the uncertainties derived in a joint MCMC ignoring the covariance would be too tight by order of percent). This would fall below the uncertainty floor mentioned above for our consistency tests.

The SPTpol $500\,\mathrm{deg^2}$ survey area is around nine times smaller than ACTPol's, covering only a few percent of the area used in the Planck analysis, and thus we can also neglect the Planck-SPTpol EE covariance.

There is partial overlap between the SPTpol patch and the W5 field used in the ACTPol analysis below decl. $-50°$ (compare Figure 1 of Henning et al. 2018 and Figure 2 of Choi et al. 2020). However, this overlap region is a small fraction of the total ($>4000\,\mathrm{deg^2}$) area used in the ACTPol analysis, and among the shallowest, with all the deep ACTPol fields lying at higher decl.

3.3.2. Gaussianity of Posterior Distributions

The ACTPol contours in Figure 1 display clear non-Gaussian features, which arise primarily because the nuisance parameter y_p, which controls the polarization efficiency, is assigned a broad uniform prior on [0.9, 1.1]. When fitting only to ACTPol EE data this opens up a large degeneracy with $A_s e^{-2\tau}$ and, to some extent, other parameters. In joint fits with either TT or TE spectra, or another experiment, this degeneracy is broken and y_p is tightly constrained, consistent with unity to

within 1%–2% (see Table 4 of Aiola et al. 2020, for results from joint fits to ACTPol and WMAP or Planck). For the consistency tests involving a comparison with ACTPol alone in Table 2 we therefore ran ACTPol chains fixing $y_p = 1$, which produces approximately Gaussian posteriors for the ΛCDM parameters (shown in the upper triangle of Figure 1). This yields slightly more stringent consistency tests in the sense that the additional scatter corresponding to different y_p values is not allowed.

Some small asymmetry of the one-dimensional posteriors is apparent for various parameters (not only for ACTPol) in Table 1. Given the lack of evidence for tension between the data sets in Table 2 we have not pursued additional tests attempting to account for this.

3.4. Comparison with Planck TT Constraints and Impact of Gravitational Lensing on the EE Spectrum

Comparisons between parameter constraints from the CMB temperature and E-mode fluctuations are important for checking the performance of the ΛCDM model and looking for hints of deviations. Since the Planck TT data is far more constraining than other TT results we compare the combined Planck+ACTPol+SPTpol EE parameters discussed above to the Planck TT parameters derived in conjunction with the `lowE` constraint on τ (Planck Collaboration VI 2020), rather than performing a joint TT analysis with ACT or SPT data.

Taking the EE and Planck TT constraints as independent, we find that the five-dimensional consistency test used in Table 2 yields TT-EE consistency at the 0.8σ level, with the largest single parameter difference being 1.4σ for $\Omega_b h^2$. The TT and EE spectra and parameters from the same sky area are partially correlated (evidenced by the nonzero TE spectrum). Over the multipole range accessible to Planck, however, the correlation coefficients between ΛCDM parameters from TT and their EE counterparts have magnitude 0.1 or smaller, even for ideal noiseless data (see Figures 4 and 5 of Kable et al. 2020). Given the significant noise levels in the Planck polarization data the TT and EE constraints are therefore well approximated as independent.

The Planck TT data has shown a persistent $>2\sigma$ preference for a larger-than-expected value of the phenomenological lensing amplitude parameter, A_L, when this is added as a free model parameter (see Planck Collaboration VI 2020; Efstathiou & Gratton 2019, for most recent results). This is associated with tensions between ΛCDM parameters for different multipole ranges and a preference for a closed universe when using TT data alone (e.g., Addison et al. 2016; Planck Collaboration XI 2016; Planck Collaboration Int. LI 2017; Di Valentino et al. 2020; Efstathiou & Gratton 2020; Han et al. 2021).

The Planck EE spectrum alone yields $A_L = 1.32^{+0.24}_{-0.27}$. Combining the EE data sets produces a much tighter constraint, comparable in precision to TT, but shifted to lower values:

$$A_L = 0.89 \pm 0.10 \quad (Planck\,\mathrm{EE} + \mathrm{ACTPol\ EE} + \mathrm{SPTpol\ EE} + \texttt{lowE}) \qquad (2)$$

$$A_L = 1.243 \pm 0.096 \quad (Planck\,\mathrm{TT} + \texttt{lowE}).$$

These values differ at 2.5σ, although the difference across the full parameter space (five ΛCDM parameters, as in the earlier consistency tests, plus A_L) is 1.7σ. The ΛCDM parameters are in good agreement, differing only at 0.6σ.

These results are qualitatively similar to those presented for the SPTpol TE+EE data by Henning et al. (2018), where the value of $A_L = 0.81 \pm 0.14$ fell 2.9σ low of the Planck TT constraint. Marginalizing over A_L produced good agreement for the ΛCDM parameters from Planck TT and SPTpol, however, which were in mild tension for $A_L = 1$.

Aiola et al. (2020) reported $A_L = 1.01 \pm 0.10$ for the ACTPol spectra (TT+TE+EE), and combining ACTPol and WMAP likewise resulted in a value centered around unity. Story et al. (2013) reported $A_L = 0.86^{+0.15}_{-0.13}$ from a joint fit to WMAP and the SPT TT spectrum. We find $A_L = 1.18 \pm 0.15$ from a similar joint fit to WMAP and ACTPol TT.

Overall, current EE measurements are consistent with the ΛCDM results from the Planck TT data, and do not show the same preference for $A_L > 1$. The exact origin of the Planck TT A_L behavior is unclear, and it may well have no connection to any underlying physics (see also, e.g., Couchot et al. 2017; Efstathiou & Gratton 2019). Any modified cosmology models that do attempt to address the TT A_L issue should also be tested against the EE data from Planck, ACTPol, and SPTpol, however, given that Planck EE provides a far weaker A_L constraint than the combination.

3.5. Choice of Prior on Optical Depth

The results shown in this work adopt the `lowE` Planck likelihood to constrain τ, based on a cross-correlation analysis of Planck High Frequency Instrument (HFI) 100 and 143 GHz data, using 30 and 353 GHz maps to clean the Galactic synchrotron and dust (see Section 2.2 of Planck Collaboration V 2020, for more details). In recent years, a number of other studies have constrained τ using different combinations of Planck and WMAP data, including alternative processing and mapmaking for the Planck polarization (e.g., Weiland et al. 2018; Planck Collaboration Int. LVII., 2020; BeyondPlanck Collaboration I 2020; Natale et al. 2020). These analyses give a spread in mean values of τ from 0.05 to 0.07, and 1σ uncertainties from 0.006 to 0.2. The `lowE` likelihood gives $\tau = 0.0506 \pm 0.0086$ (Planck Collaboration VI 2020). We also ran MCMC chains instead using a Gaussian prior $\tau = 0.065 \pm 0.015$, matching the choice adopted in the ACTPol analysis by Aiola et al. (2020). We found that for the EE results shown in Table 1 the impact of this choice is very small, with shifts in posterior means at the 0.1σ level, and changes in 68% interval bounds only at the few percent level.

4. Conclusions

We have examined the ΛCDM parameter constraints from separate and joint fits to EE power spectra from the Planck, ACTPol, and SPTpol surveys, motivated by the recent observation that the EE spectra from each experiment separately produce higher values of H_0 than, for example, Planck TT, in good agreement with the Cepheid-SNe SH0ES ladder (Dutcher et al. 2021).

A joint fit to Planck, ACTPol, and SPTpol EE spectra yields $H_0 = 68.7 \pm 1.3\ \mathrm{km\,s^{-1}\,Mpc^{-1}}$. This value is 2.4σ lower than the distance ladder, and also lower than the result from any of the data sets separately. This behavior arises from different degeneracy directions across the full ΛCDM parameter space, particularly for $\Omega_b h^2$ and n_s. We found, however, that the EE spectra from the different experiments produce consistent ΛCDM parameters, with differences across the five-dimensional parameter space (excluding τ) at the 1.4σ level or lower (Table 2). In other words, the shift to a lower H_0 is not because

the data sets are incompatible. There is a 2.5σ tension in values of the power spectrum amplitude, $A_s e^{-2\tau}$, inferred from Planck EE and SPTpol EE, which may hint at some calibration issues.

The ΛCDM parameters from the joint EE fit are consistent with the ΛCDM parameters from the Planck TT data within 0.8σ. We found that the EE data precisely constrain the phenomenological lensing amplitude parameter A_L, preferring a value consistent with unity, $A_L = 0.89 \pm 0.10$. Like earlier analyses of the ACTPol and SPTpol data we do not reproduce the preference for $A_L > 1$ seen in the Planck TT spectrum.

Based on our results, the preference for higher H_0 values from the separate EE measurements seems more likely to be due to chance fluctuations than the first hint of systematic differences in preferred parameters from, for example, the TT data. Such differences could still exist, of course, and will no doubt be the subject of future work with upcoming data. New theoretical models that impact the TT and EE spectra differently may yet be promising for resolving the Hubble disagreement. Given the consistency between the current TT and EE data within ΛCDM, however, it seems unlikely that such models would be favored over ΛCDM at a statistically significant level by CMB data.

I would like to thank Chuck Bennett for many valuable discussions, as well as comments on this work. I am also grateful to Janet Weiland, Gary Hinshaw, and Mark Halpern for helpful discussions and suggestions, and to Erminia Calabrese and Jason Hennings for help with the ACTPol and SPTpol likelihood codes.

This work was supported in part by NASA ROSES grants NNX17AF34G and 80NSSC19K0526. This work was based on observations obtained with Planck (http://www.esa.int/Planck), an ESA science mission with instruments and contributions directly funded by ESA Member States, NASA, and Canada. I acknowledge the use of the Legacy Archive for Microwave Background Data Analysis (LAMBDA), part of the High Energy Astrophysics Science Archive Center(HEASARC). HEASARC/LAMBDA is a service of the Astrophysics Science Division at the NASA Goddard Space Flight Center. This research project was conducted using computational resources at the Maryland Advanced Research Computing Center (MARCC).

Software: GetDist v1.1.2 (Lewis 2019), NumPy v1.19.5 (van der Walt et al. 2011), Matplotlib v3.3.3 (Hunter 2007), SciPy v1.6.0 (Virtanen et al. 2020).

ORCID iDs

Graeme E. Addison https://orcid.org/0000-0002-2147-2248

References

Abazajian, K., Addison, G., Adshead, P., et al. 2019, arXiv:1907.04473
Addison, G. E., Huang, Y., Watts, D. J., et al. 2016, ApJ, 818, 132
Addison, G. E., Watts, D. J., Bennett, C. L., et al. 2018, ApJ, 853, 119
Ade, P., Aguirre, J., Ahmed, Z., et al. 2019, JCAP, 2019, 056
Aiola, S., Calabrese, E., Maurin, L., et al. 2020, JCAP, 2020, 047
Aubourg, É, Bailey, S., Bautista, J. E., et al. 2015, PhRvD, 92, 123516
Austermann, J. E., Aird, K. A., Beall, J. A., et al. 2012, Proc. SPIE, 8452, 84521E
Bennett, C. L., Larson, D., Weiland, J. L., et al. 2013, ApJS, 208, 20
Benson, B. A., Ade, P. A. R., Ahmed, Z., et al. 2014, Proc. SPIE, 9153, 91531P
BeyondPlanck Collaboration I 2020, arXiv:2011.05609
Birrer, S., Shajib, A. J., Galan, A., et al. 2020, A&A, 643, A165
Blakeslee, J. P., Jensen, J. B., Ma, C.-P., Milne, P. A., & Greene, J. E. 2021, arXiv:2101.02221
Choi, S. K., Hasselfield, M., Ho, S.-P. P., et al. 2020, JCAP, 2020, 045
Couchot, F., Henrot-Versillé, S., Perdereau, O., et al. 2017, A&A, 597, A126
Di Valentino, E., Melchiorri, A., & Silk, J. 2020, NatAs, 4, 196
Dutcher, D., Balkenhol, L., Ade, P. A. R., et al. 2021, arXiv:2101.01684
eBOSS Collaboration 2020, arXiv:2007.08991
Efstathiou, G., & Gratton, S. 2019, arXiv:1910.00483
Efstathiou, G., & Gratton, S. 2020, MNRAS, 496, L91
Fields, B. D., Olive, K. A., Yeh, T.-H., Yeh, T.-H., & Young, C. 2020, JCAP, 2020, 010
Freedman, W. L., Madore, B. F., Hatt, D., et al. 2019, ApJ, 882, 34
Galli, S., Benabed, K., Bouchet, F., et al. 2014, PhRvD, 90, 063504
Gelman, A., & Rubin, D. B. 1992, StaSc, 7, 457
Han, T., Ma, Y., & Xie, K. 2021, PhRvD, 103, L041301
Henderson, S. W., Allison, R., Austermann, J., et al. 2016, JLTP, 184, 772
Henning, J. W., Sayre, J. T., Reichardt, C. L., et al. 2018, ApJ, 852, 97
Howlett, C., Lewis, A., Hall, A., & Challinor, A. 2012, JCAP, 1204, 027
Hunter, J. D. 2007, CSE, 9, 90
Kable, J. A., Addison, G. E., & Bennett, C. L. 2020, ApJ, 888, 26
Knox, L., & Millea, M. 2020, PhRvD, 101, 043533
Kosowsky, A., Milosavljevic, M., & Jimenez, R. 2002, PhRvD, 66, 063007
Kourkchi, E., Tully, R. B., Eftekharzadeh, S., et al. 2020, ApJ, 902, 145
Lewis, A. 2013, PhRvD, 87, 103529
Lewis, A. 2019, arXiv:1910.13970
Lewis, A., & Bridle, S. 2002, PhRvD, 66, 103511
Lewis, A., Challinor, A., & Lasenby, A. 2000, ApJ, 538, 473
Natale, U., Pagano, L., Lattanzi, M., et al. 2020, A&A, 644, A32
Planck Collaboration XI 2016, A&A, 594, A11
Planck Collaboration V 2020, A&A, 641, A5
Planck Collaboration VI 2020, A&A, 641, A6
Planck Collaboration Int. LI 2017, A&A, 607, A95
Planck Collaboration Int. LVII. 2020, A&A, 643, A42
Raveri, M., & Hu, W. 2019, PhRvD, 99, 043506
Riess, A. G., Casertano, S., Yuan, W., et al. 2021, ApJL, 908, L6
Schombert, J., McGaugh, S., & Lelli, F. 2020, AJ, 160, 71
Soltis, J., Casertano, S., & Riess, A. G. 2021, ApJL, 908, L5
Story, K. T., Reichardt, C. L., Hou, Z., et al. 2013, ApJ, 779, 86
Thornton, R. J., Ade, P. A. R., Aiola, S., et al. 2016, ApJS, 227, 21
van der Walt, S., Colbert, S. C., & Varoquaux, G. 2011, CSE, 13, 22
Virtanen, P., Gommers, R., Oliphant, T. E., et al. 2020, NatMe, 17, 261
Weiland, J. L., Osumi, K., Addison, G. E., et al. 2018, ApJ, 863, 161
Wong, K. C., Suyu, S. H., Chen, G. C. F., et al. 2020, MNRAS, 498, 1420